Solution-Processible 2,2′-Dimethyl-biphenyl Cored Carbazole Dendrimers as Universal Hosts for Efficient Blue, Green, and Red Phosphorescent OLEDs

Xingdong Wang, Shumeng Wang, Zhihua Ma, Junqiao Ding, Lixiang Wang,* Xiabin Jing, and Fosong Wang*

A series of solution-processible 2,2′-dimethyl-biphenyl cored dendrimers, namely G1MP, G2MP, and G3MP, is designed and synthesized by tuning the generation of periphery carbazole dendron. The resulting dendrimers all show excellent solubility in common organic solvents, and their high-quality thin films can be formed via spin-coating with a root-mean-square roughness in the range of 0.38–0.54 nm. G3MP, which contains the third-generation carbazole dendron, has the greatest potential among those made here as an ideal universal host for multicolored triplet emitters. G3MP exhibits good thermal stability, with a glass transition temperature of 368 °C, a triplet energy as high as 2.85 eV enough to prevent the loss of triplet excitons, and suitable HOMO/LUMO levels of –5.30/–2.11 eV to facilitate both hole and electron injection and transport. When using G3MP as the host, highly efficient deep-blue, blue, green, and red phosphorescent organic light-emitting diodes (PhOLEDs) are successfully demonstrated, revealing a maximum luminous efficiency up to 18.2, 28.2, 54.0, and 12.7 cd A^{-1} with the corresponding Commission Internationale de L'Eclairage (CIE) coordinates of (0.15, 0.23), (0.15, 0.35), (0.38, 0.59), and (0.64, 0.34), respectively. The state-of-art performance indicates that dendritic hosts have a favorable prospect of applications in solution-processed white PhOLEDs and full-color displays.

1. Introduction

Phosphorescent organic light-emitting diodes (PhOLEDs) with transition-metal complexes as triplet emitters have attracted much attention since they can realize nearly 100% internal quantum efficiency by harvesting both singlet and triplet excitons.[1] In most cases, these phosphors are dispersed into an appropriate host matrix to constitute the emitting layer (EML) owing to their intrinsic self-quenching and triplet–triplet annihilation.[2] Therefore, a single-host strategy has recently been proposed to prepare high-performance white PhOLEDs.[3] To generate white light, different triplet emitters are distributed in multiple regions within a single-host system, which reduces structural heterogeneity and facilitates charge injection and transport between different emissive centers. From this point of view, it is necessary to develop universal host materials that can be utilized simultaneously for blue, green, and red phosphors. However, the development of such universal hosts is a great challenge. On one hand, for blue phosphors the host's triplet energy should be at least 2.75 eV[4] so that triplet excitons can be effectively confined on the blue phosphor to avoid their loss. On the other hand, for a green or red phosphor, high triplet energy may not be required in the host because the enhancement of the triplet energy would inevitably increase the HOMO–LUMO energy gap, leading to large barriers for charge injection.[5] Hence a small exchange energy (or singlet–triplet energy difference) must be achieved in a universal host to alleviate this problem.

Until now, a number of small-molecular universal hosts have been intensively explored for the fabrication of efficient blue, green, and red PhOLEDs.[6] These small molecules need to be deposited by vacuum thermal evaporation, which may necessitate complicated technological processes, unavoidable material waste, and thus relatively high production costs. Solution processes, such as spin-coating and ink-jet printing, are desirable for low-cost, large-area full-color flat-panel displays and solid-state lighting.[7] To date, solution-processed PhOLEDs have been produced mainly from polymeric hosts codoped with phosphors by physical blending[8] or chemical bonding.[9] Unfortunately, the multidisperse molecular structures that include some defects such as random sequences, end groups, and catalyst residue may limit their device efficiencies and practical applications. Importantly, most polymers could not be used as ideal universal hosts, for it is difficult to synergistically tune the triplet energy and HOMO/LUMO levels due to the large singlet–triplet splitting in polymers.[10]

X. Wang, S. Wang, Dr. Z. Ma, Dr. J. Ding, Prof. L. Wang, Prof. X. Jing, Prof. F. Wang
State Key Laboratory of Polymer Physics and Chemistry
Changchun Institute of Applied Chemistry
Chinese Academy of Sciences
Changchun 130022, PR China
E-mail: junqiaod@ciac.ac.cn; lixiang@ciac.ac.cn
X. Wang, S. Wang
University of the Chinese Academy of Sciences
Beijing 100049, PR China

DOI: 10.1002/adfm.201302849

As an alternative, dendrimers with well-defined structures, high levels of purity, and good solubility are expected to be promising solution-processible hosts.[11] In 2009, our group firstly reported carbazole-based dendritic hosts for blue-emitting iridium(III) [bis(4,6-difluorophenyl)-pyridinato-N,C^2]-picolinate (FIrpic), and attained a power efficiency up to 15.4 lm W^{-1} (27.6 cd A^{-1}, 12.7%).[12] Compared with poly(9-vinylcarbazole) (PVK), the efficiency was improved by about 86%, which is indicative of the advantage of dendritic hosts over polymeric ones. Subsequently, Qiu and co-workers further synthesized some star-shaped dendrimers based on carbazole moieties with high triplet energy (2.86 eV), giving a maximum luminous efficiency of 25.7 cd A^{-1} for blue and 10.9 cd A^{-1} for deep-blue PhOLEDs.[13] Moreover, with a lower-triplet-energy carbazole dendrimer (2.60 eV) as the host, efficient green (38.7 cd A^{-1}) and orange (32.2 cd A^{-1}) devices were also fabricated.[14] Despite the great progress that has been made in this field, there is no report on dendrimers serving as universal hosts for multicolor triplet emitters.

Herein, we demonstrate universal dendritic hosts by incorporating 2,2′-dimethyl-biphenyl as the core to bridge carbazole dendrons for the construction of dendrimers G1MP, G2MP, and G3MP (**Scheme 1**). Herein the 2,2′-dimethyl-biphenyl core is selected because the introduction of two methyl groups into the biphenyl unit of 4,4′-bis(9-carbazolyl)-2,2′-biphenyl (CBP) is an effective way to increase triplet energy.[15] In addition, the generation of oligocarbazole is changed to adjust the HOMO/LUMO levels and film morphologies. Consequently, a high triplet energy and at the same time suitable HOMO/LUMO levels for efficient charge injection have been realized in G3MP, which contains the third-generation carbazole dendron, because of its low singlet–triplet energy difference of 0.33 eV. When using G3MP as the host, our devices reveal state-of-art luminous efficiencies of 18.2, 28.2, 54.0, and 12.7 cd A^{-1}, and Commission Internationale de L'Eclairage (CIE) coordinates of (0.15, 0.23), (0.15, 0.35), (0.38, 0.59), and (0.64, 0.34) for deep-blue, blue, green, and red electrophosphorescence, respectively. To our knowledge, this is the first report that carbazole dendrimers can be utilized as efficient universal hosts for a wide color range of phosphors from deep blue to red.

2. Results and Discussion

2.1. Synthesis and Characterization

As depicted in Scheme 1, a convergent method was adopted to synthesize dendrimers G1MP–G3MP. Initially, the first, second, and third generation carbazole dendrons D1–D3 were prepared according to previous procedures.[16] Then these dendrons were treated with 4,4′-diiodo-2,2′-dimethyl-biphenyl

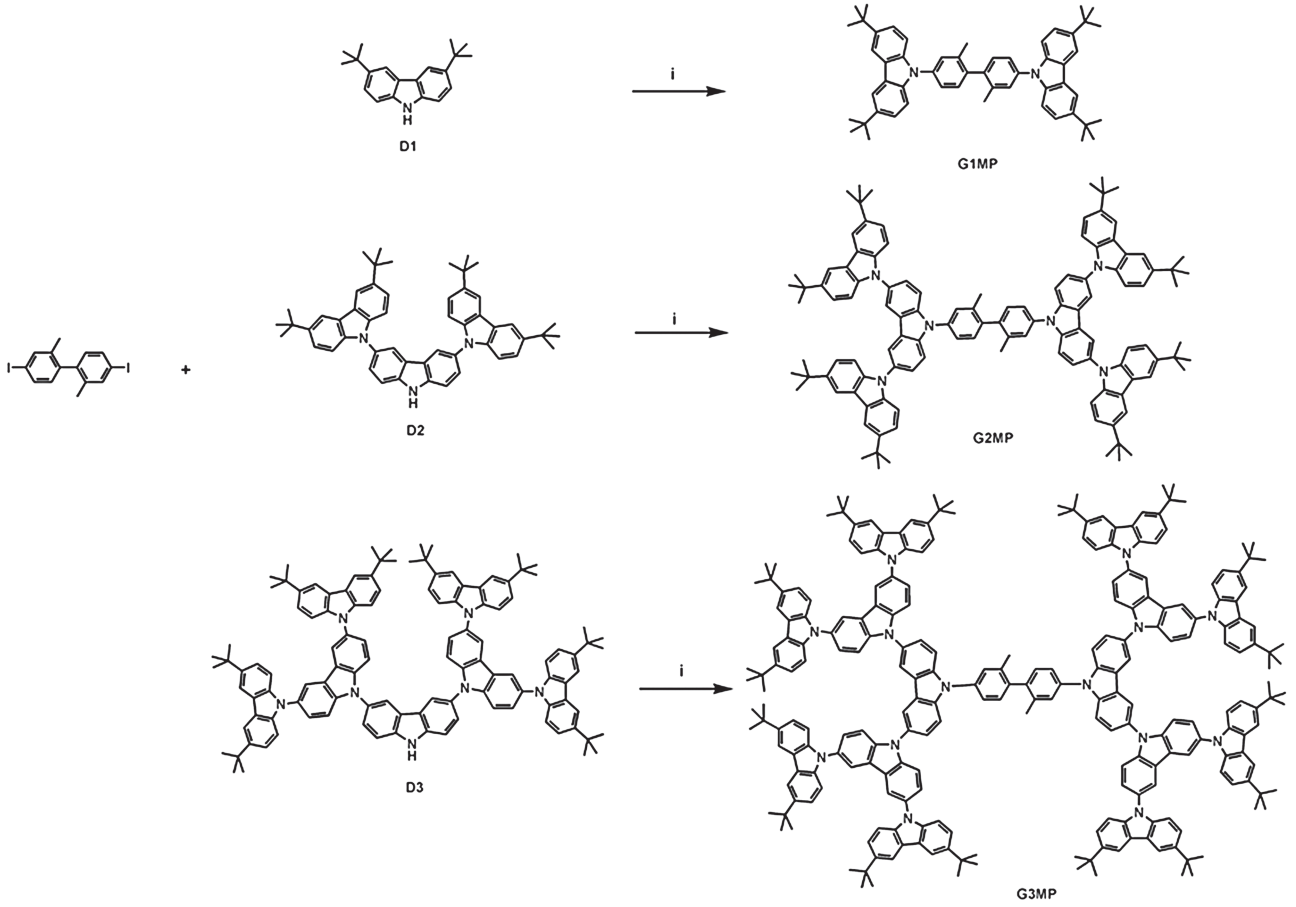

Scheme 1. Synthesis of the dendritic hosts G1MP-G3MP. Reagents and conditions: (i) K_2CO_3, CuI/Cu, *N,N*′-dimethylethyleneurea (DMI), 190 °C, 24 h.

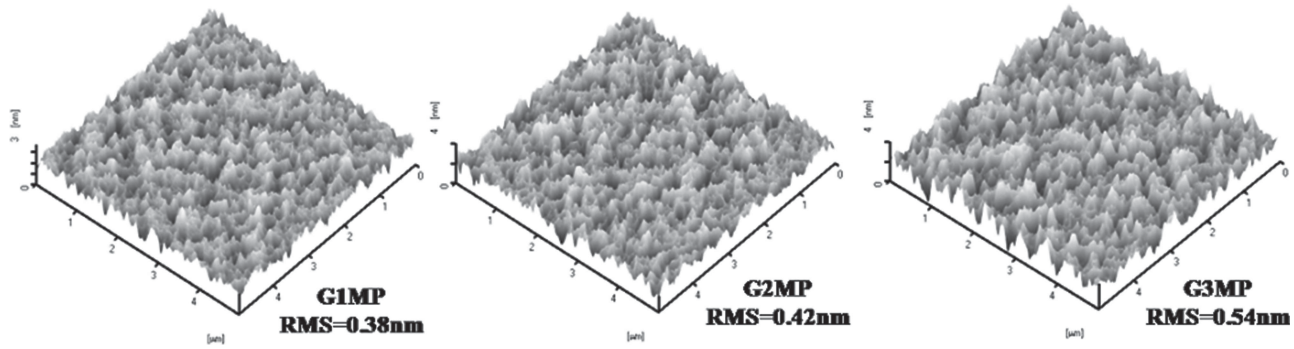

Figure 1. 3D AFM topographic images of G1MP–G3MP films. These films were prepared through spin-coating from chlorobenzene solutions onto indium tin oxide/poly(3,4-ethylenedioxythiophene):poly(styrenesulfonate) (ITO/PEDOT:PSS), and then heated at 100 °C for 30 min.

via Cu/CuI-catalyzed Ullmann reactions to afford the dendritic hosts G1MP, G2MP, and G3MP in moderate yields of 52%–69%. The obtained dendrimers could be easily and satisfactorily purified by column chromatography, and their chemical structures were confirmed by using ^{1}H NMR and ^{13}C NMR spectroscopy, mass spectrometry, and elemental analysis. Furthermore, the decoration of the dendrimer exteriors with *tert*-butyl groups ensures that all the dendrimers have good solubility in common organic solvents,[12–14,17] such as dichloromethane, cyclohexane, tetrahydrofuran, toluene, and chlorobenzene. Accordingly, high-quality thin films of the dendrimers with quite smooth and pinhole-free surfaces can be formed through spin-coating, showing root-mean-square (RMS) roughness of 0.38–0.54 nm in the atomic force microscopy (AFM) topographic images for dendrimers G1MP–G3MP (**Figure 1**).

2.2. Thermal Properties

The thermal properties of dendrimers were investigated by using thermogravimetric analysis (TGA) and differential scanning calorimetry (DSC) at a scanning rate of 10 °C min^{-1} under a nitrogen atmosphere. **Figure 2** presents the TGA and DSC curves of G1MP–G3MP. The decomposition temperature (T_d) corresponding to a 5% weight loss is 395 °C for G1MP, while G2MP and G3MP possess T_d values as high as 510 °C and 515 °C, respectively. Compared with G1MP, an enhancement of about 115–120 °C is obtained in the higher-generation dendrimers, which arises from the high molecular weight and bulky carbazole dendrons. As can be clearly seen in Figure 2b, distinct endothermic peaks related to the glass transition appear at 297 °C and 368 °C for G2MP and G3MP, respectively, which are among the highest ever reported for host materials.[14,18] This result implies that the films of G2MP and G3MP would have excellent morphological stability, a favorable feature for the realization of long-term PhOLEDs.

2.3. Photophysical Properties

The UV-vis absorption, photoluminescent (PL), and phosphorescent spectra of dendrimers G1MP–G3MP are shown in **Figure 3**, and their photophysical properties are summarized in **Table 1**. As presented in Figure 3a, G1MP–G3MP display similar patterns with three main absorption peaks, which can be attributed to the π–π^* transition of the dendrimers. The molar absorption coefficiency increases monotonically with increasing dendron generation. On going from G1MP to G2MP, the emission maxima is red-shifted by about 27 nm, which is indicative of the enlargement of the conjugation length. By contrast,

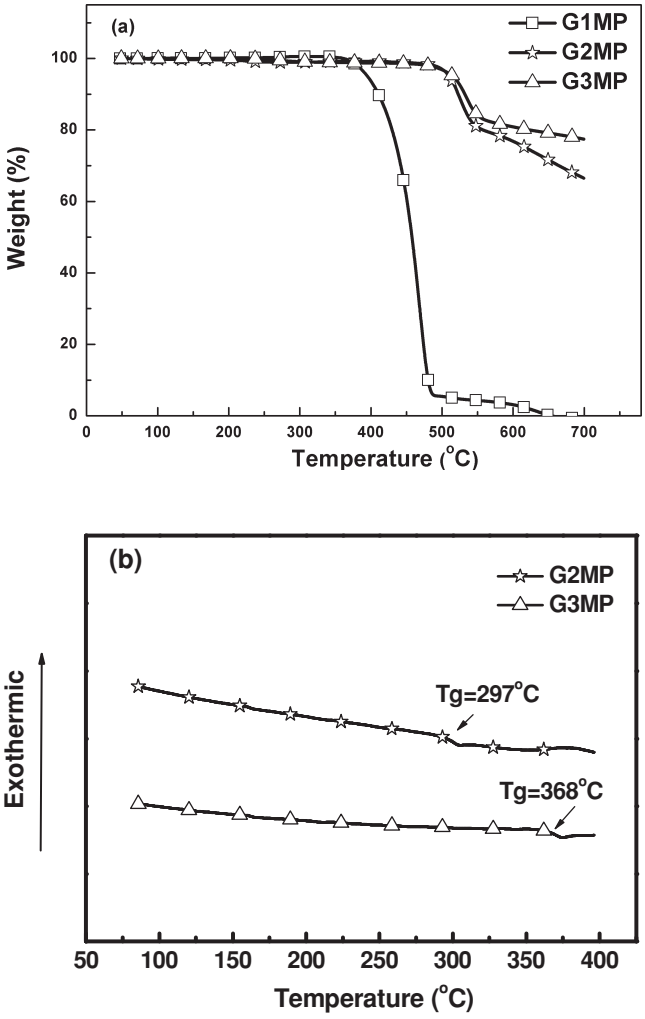

Figure 2. a) TGA traces of dendrimers G1MP–G3MP and b) DSC curves of G2MP and G3MP measured at a heating rate of 10 °C min^{-1} under N_2.

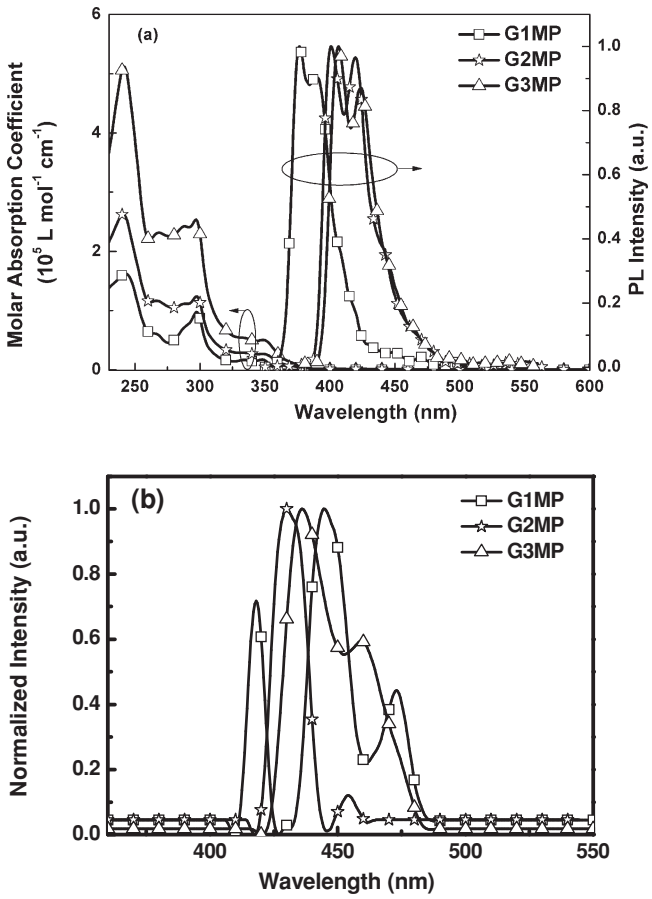

Figure 3. a) Absorption spectra in CH_2Cl_2 (5×10^{-6} M) and PL spectra in toluene (5×10^{-4} M) for dendrimers G1MP–G3MP; b) phosphorescent spectra of dendrimers G1MP–G3MP in toluene (5×10^{-4} M) at 77 K.

a bathochromic shift of only 3 nm is observed from G2MP to G3MP, which suggests that the delocalization of the excited states is mainly confined to the second-generation dendrons and does not obviously extend to the third-generation ones.

From the highest energy 0–0 vibration peaks of the phosphorescent spectra at 77 K in Figure 3b, the estimated triplet energy is lowered from G1MP to G3MP, in agreement with the variation tendency of their PL spectra at 298 K. For G3MP, although an about 0.13 eV decrease is found relative to G1MP, its triplet energy is sufficient to prevent triplet energy back-transfer[19] when serving as the host for [bis(3,5-difluoro-4-cyanophenyl)-pyridine] iridium picolinate (FCNIrpic, 2.74 eV),[20] FIrpic (2.62 eV),[21] G0 (2.44 eV)[22] and $(TPAPQ)_2Ir(acac)$ (2.11 eV; TPAPQ=*N,N*-diphenyl-*N*-[4-(4-phenyl-quinol-2-yl)-phenyl]-amine).[23] Additionally, G1MP–G3MP show much higher triplet energies than dendrimers with a biphenyl core (2.60 – 2.62 eV),[14] which indicates that the presence of two methyl groups here plays a crucial role in retaining high triplet energy.

2.4. Electrochemical Properties

Cyclic voltammetry (CV) was performed in CH_2Cl_2 to examine the electrochemical properties of the dendrimers with ferrocene/ferrocenium (Fc/Fc^+) as the internal standard. During the anodic sweeping, G1MP–G3MP exhibit reversible oxidation processes (**Figure 4**), whereas no reduction signals are detected upon the cathodic scan. As the dendron grows, the first oxidation wave shifts towards a negative potential that results from the much richer electron-cloud density of the higher-generation dendrimer. Correspondingly, the HOMO level increases from G1MP to G2MP and G3MP. In comparison to G1MP, it is worth noting that both the hole- and electron-injection barriers are reduced by about 0.13–0.14 eV for G3MP. Appropriate HOMO/LUMO levels for efficient carrier injection and high triplet energy have been realized simultaneously in G3MP. This specification is not reachable for most π-conjugated molecules and polymers whose exchange energy is larger than 0.5 eV.[5a,10] The reason is that G3MP has a low exchange energy (Table 1), which is caused by the more separated HOMO/LUMO distribution with increased dendron generation as shown in Figure S5.[24] Given this consideration, G3MP is thereby expected to have a great potential as a universal host for blue, green, and red phosphors.

2.5. Electroluminescent Properties of PhOLEDs

With these newly synthesized dendrimers in hand, we fabricated FIrpic-based blue PhOLEDs. The structure of devices A1–A3 is ITO/PEDOT:PSS (40 nm)/G1MP–G3MP:FIrpic

Table 1. Physical data of the dendrimers.

Dendrimer	λ_{abs} (log ε)[a)] [nm]	ΔE_g[b)] [eV]	λ_{em}[c)] [nm]	E_S[d)] [eV]	E_T[e)] [eV]	ΔE_{ST}[f)] [eV]	HOMO[g)] [eV]	LUMO[g)] [eV]	T_g [°C]	T_d[h)] [°C]
G1MP	242 (4.8), 297 (4.6), 349 (3.8)	3.46	368	3.47	2.98	0.49	–5.44	–1.98	—	395
G2MP	242 (5.4), 297 (5.1), 349 (4.4)	3.21	395	3.23	2.89	0.34	–5.31	–2.10	297	510
G3MP	242 (5.7), 297 (5.4), 349 (4.7)	3.19	398	3.18	2.85	0.33	–5.30	–2.11	368	515

[a)]Measured in CH_2Cl_2 solution (5×10^{-6} M) at 298 K; [b)]Calculated from the onset of the absorption in CH_2Cl_2; [c)] Measured in toluene solution (5×10^{-4} M) at 298 K; [d)] Estimated from the highest energy vibronic band of the fluorescent spectra at 77 K; [e)] Estimated from the highest energy vibronic band of the phosphorescent spectra at 77 K; [f)]The exchange energy was estimated from the difference between singlet (E_S) and triplet energies (E_T); [g)] The HOMO and LUMO levels are calculated as described in the Experimental Section; [h)] The decomposition temperature corresponding to a 5% weight loss.

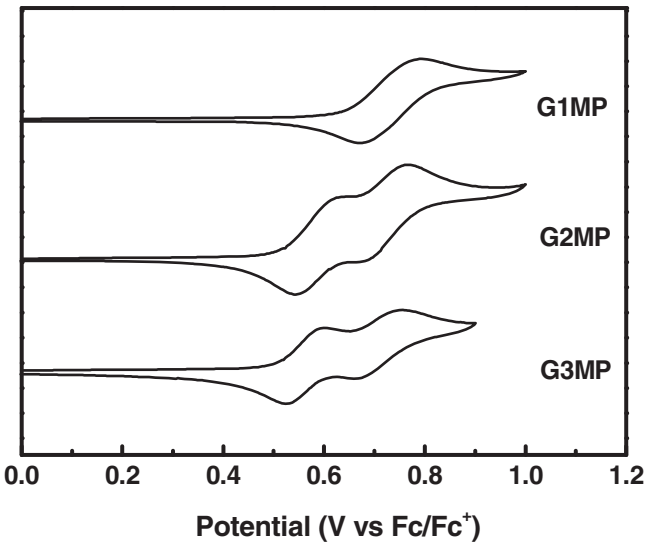

Figure 4. Cyclic voltammograms of the dendrimers, measured in CH_2Cl_2 at a scan rate of 100 mV s^{-1}.

(15 wt%, 35 nm)/SPPO13 (65 nm)/LiF (0.5 nm)/Al (100 nm), where 2,7-bis(diphenylphosphoryl)-9,9′-spirobi[fluorene] (SPPO13) acts as the electron-transporting and hole-blocking material (**Figure 5**).[25] **Figure 6**a and b show the current density–voltage–brightness (*J–V–L*) characteristics and efficiencies as a function of current density for the devices, and the electroluminescent (EL) data are tabulated in **Table 2**. The *J–V* curve is found to shift to lower voltages, and the turn-on voltages decrease from A1 to A3. Meanwhile, both the current density and luminance of the corresponding device at a given voltage increase regularly with the generation number. These observations may be ascribed to the improved charge balance caused by the following two aspects: i) as discussed above, the elevated HOMO and lowered LUMO levels of G3MP can favor both the hole and electron injection; and ii) as demonstrated by the hole-only devices (Figure S6), the hole-transport capability of G3MP seems to be larger than those of G1MP and G2MP, which correlates well with the *J–V* curves of devices A1–A3. As a result, device A3 hosted by G3MP displays performance values that are comparable to those of previously developed dendritic hosts (Table 2).[12,13]

As shown in Figure 6c, the EL spectra of devices A1–A3 all exhibit blue emission at around 472 nm that is characteristic of FIrpic, and no residual emission from G1MP, G2MP, or G3MP is detected. This result demonstrates that complete energy transfer can occur from hosts G1MP–G3MP to FIrpic because there is a good overlap between the PL spectra of G1MP–G3MP and the absorption spectrum of FIrpic (Figure S7). Moreover, the CIE coordinates vary slightly from device A1 to device A3, caused by the recombination zone shift in devices owing to the different charge transport capabilities of the dendritic hosts.[26]

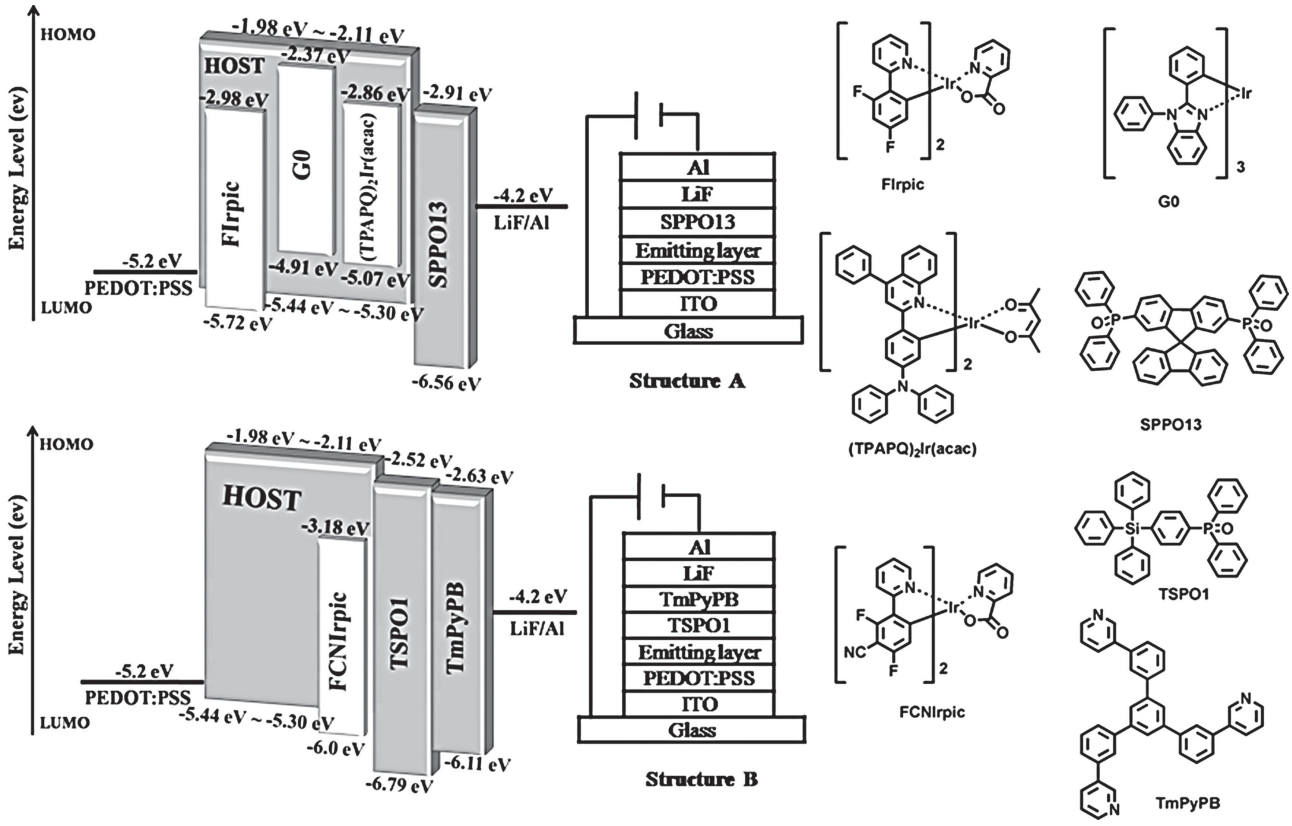

Figure 5. Schematic diagram of the EL device configurations, molecular structures of the materials used in these devices, and their corresponding energy levels.

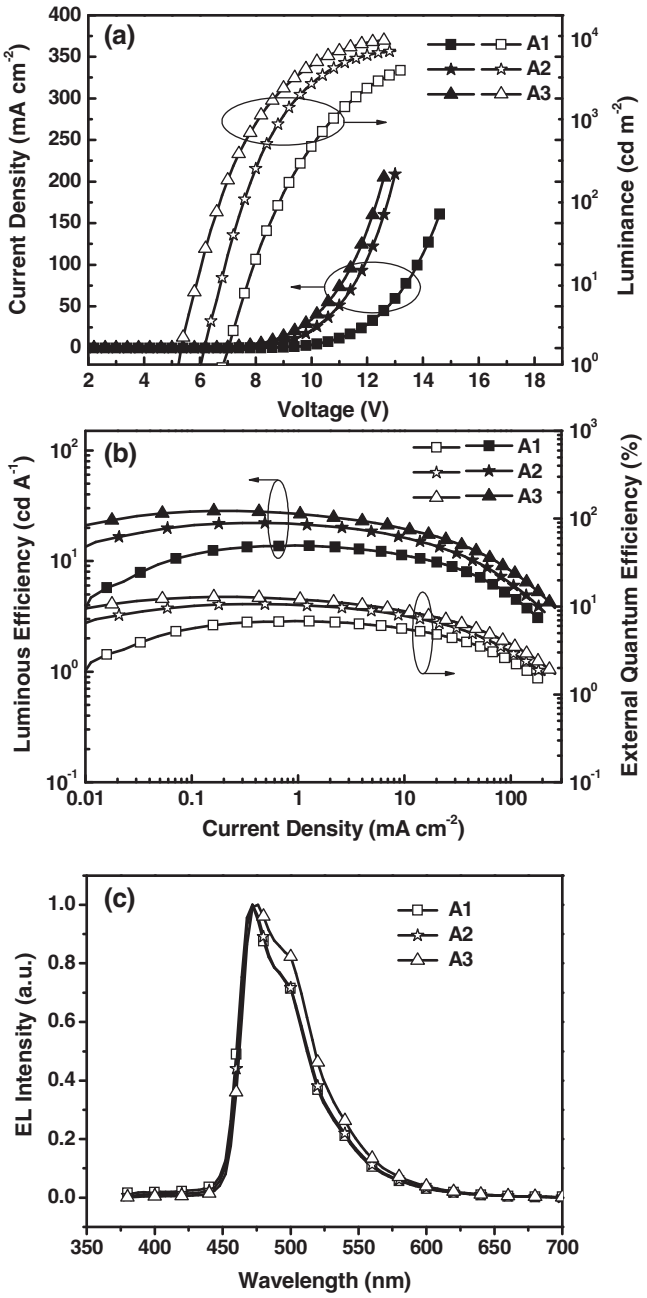

Figure 6. a) *J–V–L* characteristics, b) luminous efficiency and external quantum efficiency as a function of current density, and c) EL spectra at 1000 cd m^{-2} for devices A1–A3.

To evalute the possibility of using these dendrimers as hosts for deep-blue PhOLEDs, FCNIrpic was chosen as the dopant to prepare devices B1–B3 with the configuration of ITO/PEDOT:PSS (40 nm)/G1MP–G3MP:FCNIrpic (10 wt%, 35 nm)/TSPO1 (8 nm)/TmPyPB (52 nm)/LiF (0.5 nm)/Al (100 nm) (Figure 5). In this case, diphenylphosphine oxide-4-(triphenylsilyl)phenyl (TSPO1)[27] instead of SPPO13 was applied as the electron-transporting and hole-blocking material due to its higher triplet energy (3.36 eV) and deeper HOMO level (–6.79 eV) than SPPO13 (E_T: 2.73 eV; HOMO: –6.56 eV); 1,3,5-tri(*m*-pyrid-3-yl-phenyl)benzene (TmPyPB) acted as the electron-transporting material because its electron mobility may reach to 1.0×10^{-3} cm^2 V^{-1} s^{-1};[28] and the combination of an analogue of TSPO1 and TmPyPB can realize high-performance deep-blue electrophosphorescence.[29] The same trends are observed for devices B1–B3 as for A1–A3. For example, the turn-on voltage decreases from device B1 to B3, as does the efficiency enhancement (**Figure 7**). Among these devices, device B3 with G3MP as the host thereby achieves the best device performance. Compared with star-shaped dendritic hosts ($\eta_{ext,\,max}$: 5.1%; CIE: (0.18, 0.25)),[13] an about two-fold improvement is obtained associated with slightly better CIE coordinates.

Based on the fact that G3MP performs the best among G1MP–G3MP in blue and deep-blue devices, we next used G3MP as the host for green phosphor G0 and red phosphor $(TPAPQ)_2Ir(acac)$ to demonstrate its versatility. The device structure was the same as that of devices A1–A3, but the EML was composed of G3MP doped with 30 wt% G0 for device A4 and 6 wt% $(TPAPQ)_2Ir(acac)$ for device A5. As indicated in **Figure 8** and Table 2, the green device A4 has an extremely low turn-on voltage. At a brightness of 1000 cd m^{-2}, the external quantum efficiency still remains as high as 13.3%, and only a loss of 16% is observed, indicative of a gentle efficiency roll-off. The performance is much higher than that of dendrimers that contain a biphenyl core, which show $\eta_{l,\,max}$ of 38.7 cd A^{-1}, $\eta_{p,\,max}$ of 15.7 lm W^{-1} and $\eta_{ext,\,max}$ of 11.4%. It should be noted that the red device A5 turns on at a higher voltage than does device A4. Different from $(TPAPQ)_2Ir(acac)$, G0 could contribute to the effective hole-injection/transporting in device A4 due to its shallow HOMO level (–4.91 eV) and high doping concentration (30 wt%). Therefore, some excitons may be formed directly on G0, resulting in the reduction of driving voltage.[30] In spite of this large turn-on voltage, device A5 exhibits excellent performance characteristics.

3. Conclusions

We have designed and synthesized a novel series of solution-processible carbazole-based dendritic host materials by incorporating 2,2′-dimethyl-biphenyl as the core. With the increasing dendron generation, G3MP achieves a tradeoff between high triplet energy and appropriate HOMO/LUMO levels, which is suitable for a wide color range of phosphors. High-performance deep-blue, blue, green, and red PhOLEDs have been successfully realized when hosted by G3MP, showing significant efficiencies up to 18.2, 28.2, 54.0, and 12.7 cd A^{-1}, respectively. As G3MP represents the first example of a dendritic universal host, we believe that this work will promote the development of this kind of dendritic hosts over that of small molecular and polymeric counterparts, and their applications in white light-emitting devices and full-color displays.

Table 2. EL performance of blue, deep-blue, green, and red PhOLEDs.

Device	Host	Dopant	V_{on}[a)] [V]	L_{max} [cd m^{-2}]	$\eta_{l,\,max}$ [cd A^{-1}]	$\eta_{p,\,max}$ [lm W^{-1}]	$\eta_{ext,\,max}$ [%]	CIE[b)] (x, y)
A1	G1MP	FIrpic	6.9	5533	13.8	5.0	6.8	(0.15, 0.30)
A2	G2MP	FIrpic	6.1	7237	22.1	9.5	10.7	(0.15, 0.31)
A3	G3MP	FIrpic	5.3	9823	28.2	14.1	12.8	(0.15, 0.35)
B1	G1MP	FCNIrpic	7.3	1925	10.8	3.3	7.0	(0.15, 0.18)
B2	G2MP	FCNIrpic	5.5	1856	13.9	6.2	8.6	(0.15, 0.20)
B3	G3MP	FCNIrpic	4.5	2277	18.2	11.4	10.3	(0.15, 0.23)
A4	G3MP	G0	2.9	35816	54.0	48.6	15.9	(0.38, 0.59)
A5	G3MP	$(TPAPQ)_2Ir(acac)$	4.5	6985	12.7	7.4	11.0	(0.64, 0.34)

[a)] Turn-on voltage at a brightness of 1 cd m^{-2}; [b)] At a brightness of 1000 cd m^{-2}. L_{max}: maximum brightness; $\eta_{l,\,max}$: maximum luminous efficiency; $\eta_{p,\,max}$: maximum power efficiency; $\eta_{ext,\,max}$: maximum external quantum efficiency.

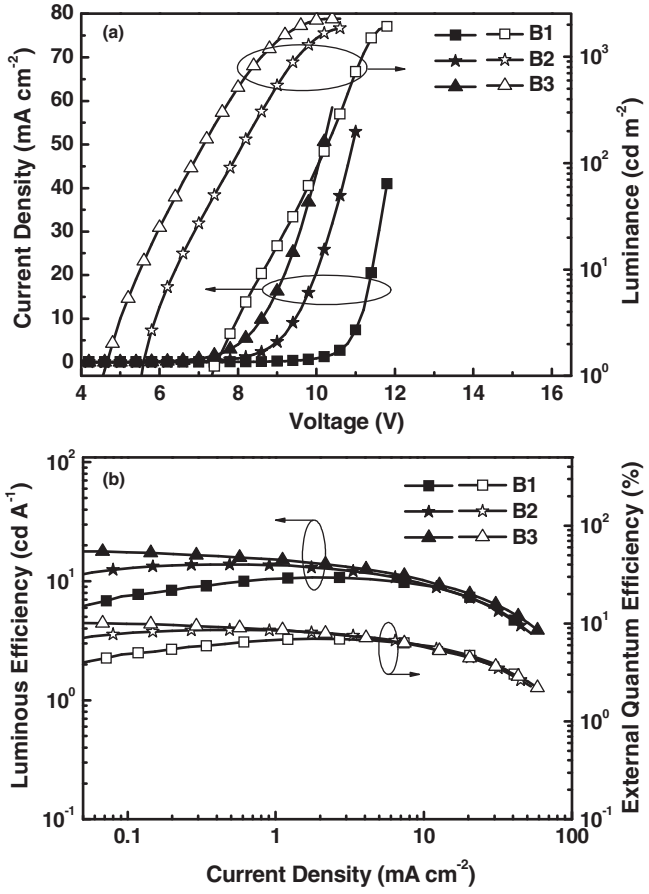

Figure 7. a) Current density–voltage–luminance (*J–V–L*) characteristics, and b) luminous efficiency and external quantum efficiency as a function of current density for devices B1–B3.

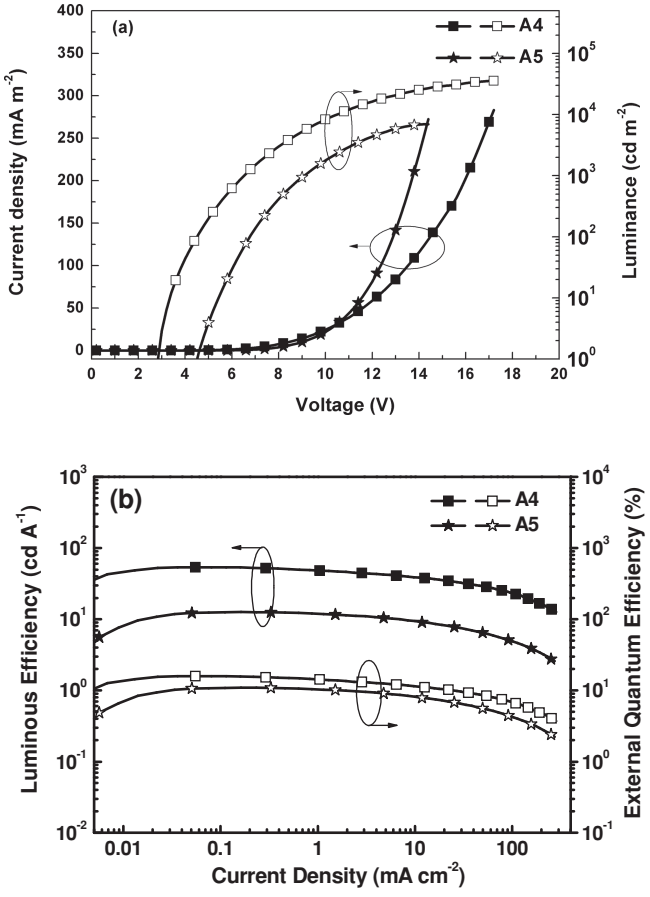

Figure 8. a) *J–V–L* characteristics, and b) luminous efficiency and external quantum efficiency as a function of current density for devices A4 and A5.

4. Experimental Section

General Information: All chemicals and reagents were used as-received from commercial sources without further purification. Solvents for chemical synthesis were purified according to the standard procedures. 4,4′-diiodo-2,2′-dimethyl-biphenyl[31] and carbazole-based dendrons including D1, D2, and D3[16] were synthesized according to the literature.

G1MP: A mixture of the first-generation carbazole dendron D1 (3.07 g, 11 mmol), 4,4′-diiodo-2,2′-dimethyl-biphenyl (2.17 g, 5 mmol), CuI (0.38 g, 2.0 mmol), copper powder (0.64 g, 10 mmol), and K_2CO_3 (4.15 g, 30 mmol) in *N,N*′-dimethylethyleneurea (DMI) (30 mL) was heated at 190 °C for 24 h under a N_2 atmosphere. The reaction mixture was cooled to room temperature, poured into water, extracted with dichloromethane, and then dried with anhydrous Na_2SO_4. After the solvent was removed, the residue was isolated by using silica gel column

chromatography (*n*-hexane/dichloromethane = 5/1, v/v) to give a white solid (2.54 g, 69%). ^{1}H NMR (300 MHz, $CDCl_3$) δ 8.16 (s, 4H), 7.51 (s, 2H), 7.47 (t, J = 4.9 Hz, 6H), 7.40 (d, J = 8.0 Hz, 2H), 2.25 (s, 6H), 1.47 (s, 36H).^{13}C NMR (300 MHz, $CDCl_3$) δ 142.87, 139.64, 139.38, 137.83, 137.40, 130.78, 127.95, 123.93, 123.64, 123.46, 116.30, 109.43, 34.81, 32.12, 20.18. MALDI-TOF (m/z): 736.5 (Calcd for $[M]^+$ 736.4). Anal. calcd for $C_{54}H_{60}N_2$: C, 87.99; H, 8.21; N, 3.80. Found: C, 87.98; H, 8.23; N, 3.75.

G2MP: This compound was prepared from D2 and 4,4′-diiodo-2,2′-dimethyl-biphenyl according to a similar procedure as G1MP. Silica gel column chromatography (cyclohexane/dichloromethane = 5/1, v/v) was applied to provide the desired product as a white solid (1.91 g, 60%). ^{1}H NMR (300 MHz, $CDCl_3$) δ 8.27 (d, J = 1.7 Hz, 4H), 8.17 (d, J = 1.5 Hz, 8H), 7.76 (t, J = 7.2 Hz, 6H), 7.72 – 7.68 (m, 2H), 7.66 (dd, J = 8.7, 1.9 Hz, 4H), 7.60 (d, J = 8.0 Hz, 2H), 7.47 (dd, J = 8.7, 1.8 Hz, 8H), 7.36 (d, J = 8.6 Hz, 8H), 2.42 (s, 6H), 1.47 (s, 72H). ^{13}C NMR (300MHz, $CDCl_3$) δ 142.68, 140.58, 140.29, 138.47, 136.70, 131.21, 131.02, 128.60, 126.10, 124.59, 124.12, 123.68, 123.26, 119.47, 116.35, 111.41, 109.22, 34.84, 32.16, 20.39. MALDI-TOF (m/z): 1621.0 (Calcd for $[M]^+$ 1620.9). Anal. calcd for $C_{118}H_{120}N_6$: C, 87.36; H, 7.46; N, 5.18. Found: C, 87.27; H, 7.71; N, 4.94.

G3MP: This compound was prepared from D3 and 4,4′-diiodo-2,2′-dimethyl-biphenyl according to a similar procedure as G1MP. Silica gel column chromatography (cyclohexane/dichloromethane = 5/1, v/v) was applied to provide the desired product as a white solid (1.78 g, 52%). ^{1}H NMR (300 MHz, $CDCl_3$) δ 8.65 (s, 4H), 8.35 (s, 8H), 8.22 (d, J = 1.2 Hz, 16H), 8.02 (d, J = 8.7 Hz, 4H), 7.95 (dd, J = 8.7, 1.4 Hz, 4H), 7.93 – 7.81 (m, 6H), 7.79 – 7.71 (m, 8H), 7.69 (dd, J = 8.8, 1.3 Hz, 8H), 7.52 (dd, J = 8.7, 1.5 Hz, 16H), 7.42 (d, J = 8.6 Hz, 16H), 2.56 (s, 3H), 1.52 (s, 144H). ^{13}C NMR (300MHz, $CDCl_3$) δ 142.64, 141.48, 141.29, 140.91, 140.30, 138.70, 136.51, 133.17, 131.37, 130.89, 130.17, 128.77, 126.52, 126.14, 124.76, 124.30, 123.90, 123.64, 123.21, 120.15, 119.53, 116.31, 112.00, 111.16, 109.18, 34.81, 32.13, 20.45. MALDI-TOF (m/z): 3390.8 (Calcd for $[M+H]^+$ 3390.9). Anal. calcd for $C_{246}H_{240}N_{14}$: C, 87.09; H, 7.13; N, 5.78. Found: C, 86.39; H, 7.50; N, 5.43.

Measurements and Characterization: ^{1}H NMR and ^{13}C NMR spectra were recorded with a Bruker Avance 300 NMR spectrometer. Elemental analysis was performed by using a Bio-Rad elemental analysis system. Matrix-assisted laser desorption ionization/time-of-flight (MALDI-TOF) mass spectra were performed on an AXIMA CFR MS apparatus (COMPACT). Thermal gravimetric analysis (TGA) and differential scanning calorimetry (DSC) were performed at a heating rate of 10 °C min^{-1} under a flow of N_2 with PerkinElmer-TGA 7 and PerkinElmer-DSC 7 system, respectively. UV-vis absorption and photoluminescence spectra at room temperature were measured by using a PerkinElmer Lambda 35 UV/Vis spectrometer and PerkinElmer LS 50B spectrofluorometer, respectively. At 77 K, both the fluorescence and phosphorescence spectra were recorded on a Perkin–Elmer LS-50B spectrofluorometer equipped with a low-temperature luminescence accessory. The samples (5×10^{-4} M in toluene) were introduced into a quartz tube (4 mm diameter) and cooled to 77 K in a liquid nitrogen bath. Dry nitrogen was circulated in the cell compartment to avoid water condensation on the cell walls. The fluorescence spectra were obtained when the apparatus was operated in a fluorescence mode excited at 350 nm. The phosphorescence spectra were obtained when the apparatus was operated in a phosphorescence mode with a delay time of 1.00 ms and a gate time of 10.00 ms under an excitation pulse of 350 nm. The highest energy peaks in the fluorescence and phosphorescence spectra at 77 K were assigned as the $S_0v^{=0} \leftarrow S_1v^{=0}$ and $S_0v^{=0} \leftarrow T_1v^{=0}$ transitions, respectively. The exchange energy was estimated from the difference between the singlet and triplet energy. AFM characterization was performed on SPA300HV with a SPI3800N controller (Seiko Instruments Inc., Japan) in a tapping mode. Cyclic voltammetry was performed on an EG&G 283 (Princeton Applied Research) potentiostat/galvanostat system at a scanning rate of 100 mV s^{-1}. The samples were tested in 1 mM CH_2Cl_2 solutions with the ferrocene/ferrocenium couple as the reference. The supporting electrolyte was 0.1 M tetrabutylammonium perchlorate (n-Bu_4NClO_4). The HOMO levels were calculated according to the equation E_{HOMO} = –e [*E*ox onset + 4.8 V], and the LUMO levels were calculated according to the equation $E_{LUMO} = E_{HOMO} + \Delta E_g$, where ΔE_g is the optical band gap estimated from the onset of the absorption spectrum. Theoretical calculations were performed using the Gaussian 03 program, and the chemical structures of G1MP–G3MP were fully optimized by means of density functional theory (DFT) using Beck's three-parameterized Lee–Yang–Parr exchange functional (B3LYP) with 6-31G* basis sets.

Device Fabrication and Testing: The indium-tin oxide (ITO) glass substrates were cleaned in an ultrasonic solvent bath, baked in a heating chamber at 120 °C, and treated with O_2 plasma for 25 min before use. A 40-nm thick ITO-modifying layer of poly(ethylenedioxythiophene):poly(styrene sulfonic acid) (PEDOT:PSS) was spin-coated on top of ITO, and then baked for 20 min at 120 °C. The emitting layer was spin-coated from a chlorobenzene solution and annealed at 100 °C for 30 min to remove the residual solvent in N_2 atmosphere. Then, for devices with structure A, a 65-nm thick SPPO13 was evaporated as the electron-transporting and hole-blocking layer at a pressure less than 4.0×10^{-4} Pa; for devices with structure B, an 8-nm thick TSPO1 and a 52-nm thick TmPyPB layer were evaporated in succession as the electron-transporting and hole-blocking layer. Finally, a 0.5-nm thick LiF and 100-nm thick Al layer were evaporated as the cathode. The active area of all the devices was 14 mm^2. The EL spectra and CIE coordinates were measured using a PR650 spectra colorimeter. The current density–voltage and brightness–voltage curves of the devices were measured using a Keithley 2400/2000 source meter and a calibrated silicon photodiode. All the measurements were carried out at room temperature under ambient conditions. The external quantum efficiencies were calculated from the brightness, current density, and EL spectrum, by assuming a Lambertian distribution. Without device encapsulation, the lifetime measurements were directly carried out under a constant current density in a glovebox.

Supporting Information

Supporting Information is available from the Wiley Online Library or from the author.

Acknowledgements

The authors are grateful to the 973 Project (2009CB623601 and 2009CB930603), National Natural Science Foundation of China (Nos. 51322308, 21174144 and 21204084), and Science Fund for Creative Research Groups (No. 20921061) for financial support of this research.

Received: August 14, 2013
Revised: December 18, 2013
Published online: February 18, 2014

[1] a) M. A. Baldo, D. F. O'Brien, Y. You, A. Shoustikov, S. Sibley, M. E. Thompson, S. R. Forrest, *Nature* **1998**, *395*, 151; b) C. Adachi, M. A. Baldo, M. E. Thompson, S. R. Forrest, *J. Appl. Phys.* **2001**, *90*, 5048.
[2] M. A. Baldo, C. Adachi, S. R. Forrest, *Phys. Rev. B* **2000**, *62*, 10967.
[3] Q. Wang, J. Ding, D. Ma, Y. Cheng, L. Wang, F. Wang, *Adv. Mater.* **2009**, *21*, 2397.
[4] a) S. Shao, J. Ding, L. Wang, X. Jing, F. Wang, *J. Am. Chem. Soc.* **2012**, *134*, 15189; b) S. Shao, J. Ding, L. Wang, X. Jing, F. Wang, *J. Am. Chem. Soc.* **2012**, *134*, 20290.
[5] a) A. van Dijken, J. J. A. M. Bastiaansen, N. M. M. Kiggen, B. M. W. Langeveld, C. Rothe, A. Monkman, I. Bach, P. Stossel, K. Brunner, *J. Am. Chem. Soc.* **2004**, *126*, 7718; b) K. Brunner,

A. van Dijken, H. Borner, J. J. A. M. Bastiaansen, N. M. M. Kiggen, B. M. W. Langeveld, *J. Am. Chem. Soc.* **2004**, *126*, 6035.

[6] a) P.-I. Shih, C.-H. Chien, F.-I. Wu, C.-F. Shu, *Adv. Funct. Mater.* **2007**, *17*, 3514; b) S. Gong, Y. Chen, J. Luo, C. Yang, C. Zhong, J. Qin, D. Ma, *Adv. Funct. Mater.* **2011**, *21*, 1168; c) H.-H. Chou, H.-H. Shih, C.-H. Cheng, *J. Mater. Chem.* **2010**, *20*, 798; d) H.-H. Chou, C.-H. Cheng, *Adv. Mater.* **2010**, *22*, 2468; e) C. Cai, S.-J. Su, T. Chiba, H. Sasabe, Y.-J. Pu, K. Nakayama, J. Kido, *Org. Electron.* **2011**, *12*, 843.

[7] a) H. Wu, L. Ying, W. Yang, Y. Cao, *Chem. Soc. Rev.* **2009**, *38*, 3391; b) M. C. Gather, A. Kohnen, K. Meerholz, *Adv. Mater.* **2011**, *23*, 233.

[8] a) C. Jiang, W. Yang, J. Peng, S. Xiao, Y. Cao, *Adv. Mater.* **2004**, *16*, 537; b) Y. Mo, R. Tian, W. Shi, Y. Cao, *Chem. Commun.* **2005**, 4925; c) F. Huang, Y.-H. Niu, Y. Zhang, J.-W. Ka, M. S. Liu, A. K.-Y. Jen, *Adv. Mater.* **2007**, *19*, 2010; d) F. Huang, P.-I. Shih, C.-F. Shu, Y. Chi, A. K.-Y. Jen, *Adv. Mater.* **2009**, *21*, 361; e) Y.-C. Chen, G.-S. Huang, C.-C. Hsiao, S.-A. Chen, *J. Am. Chem. Soc.* **2006**, *128*, 8549; f) X. H. Yang, F. Jaiser, B. Stiller, D. Neher, F. Galbrecht, U. Scherf, *Adv. Funct. Mater.* **2006**, *16*, 2156.

[9] a) X. Chen, J.-J. Liao, Y. Liang, M. O. Ahmed, H.-E. Tseng, S.-A. Chen, *J. Am. Chem. Soc.* **2003**, *125*, 636; b) J. Jiang, C. Jiang, W. Yang, H. Zhen, F. Huang, Y. Cao, *Macromolecules* **2005**, *38*, 4072; c) J. Jiang, Y. Xu, W. Yang, R. Guan, Z. Liu, H. Zhen, Y. Cao, *Adv. Mater.* **2006**, *18*, 1769; d) X.-H. Yang, F.-I. Wu, D. Neher, C.-H. Chien, C.-F. Shu, *Chem. Mater.* **2008**, *20*, 1629; e) Z. Ma, J. Ding, B. Zhang, C. Mei, Y. Cheng, Z. Xie, L. Wang, X. Jing, F. Wang, *Adv. Funct. Mater.* **2010**, *20*, 138; f) Z. Ma, L. Chen, J. Ding, L. Wang, X. Jing, F. Wang, *Adv. Mater.* **2011**, *23*, 3726.

[10] a) Y. V. Romanovskii, A. Gerhard, B. Schweitzer, U. Scherf, R. I. Personov, H. Bassler, *Phys. Rev. Lett.* **2000**, *84*, 1027; b) A. P. Monkman, H. D. Burrows, L. J. Hartwell, L. E. Horsburgh, I. Hamblett, S. Navaratnam, *Phys. Rev. Lett.* **2001**, *86*, 1358; c) H. Bassler, V. I. Arkhipov, E. V. Emelianova, A. Gerhard, A. Hayer, C. Im, J. Rissler, *Synth. Met.* **2003**, *135*, 377.

[11] a) G. R. Newkome, C. N. Moorefield, F. Vögtle, Dendritic Molecules: Concept, Synthesis and Perspectives, Wiley-VCH, Weinheim, Germany **1996**; b) T. Weil, E. Reuther, K. Müllen, *Angew. Chem. Int. Ed.* **2002**, *41*, 1900.

[12] J. Ding, B. Zhang, J. Lu, Z. Xie, L. Wang, X. Jing, F. Wang, *Adv. Mater.* **2009**, *21*, 4983.

[13] a) W. Jiang, Z. Ge, P. Cai, B. Huang, Y. Dai, Y. Sun, J. Qiao, L. Wang, L. Duan, Y. Qiu, *J. Mater. Chem.* **2012**, *22*, 12016; b) W. Jiang, J. Tang, W. Yang, X. Ban, B. Huang, Y. Dai, Y. Sun, L. Duan, J. Qiao, L. Wang, Y. Qiu, *Tetrahedron* **2012**, *68*, 5800.

[14] J. Li, T. Zhang, Y. Liang, R. Yang, *Adv. Funct. Mater.* **2013**, *23*, 619.

[15] S. Tokito, T. Iijima, Y. Suzuri, H. Kita, T. Tsuzuki, F. Sato, *Appl. Phys. Lett.* **2003**, *83*, 569.

[16] J. Ding, J. Lü, Y. Cheng, Z. Xie, L. Wang, X. Jing, F. Wang, *Adv. Funct. Mater.* **2008**, *18*, 2754.

[17] a) J. Ding, B. Wang, Z. Yue, B. Yao, Z. Xie, Y. Cheng, L. Wang, X. Jing, F. Wang, *Angew. Chem. Int. Ed.* **2009**, *48*, 6664; b) L. Chen, J. Ding, Y. Cheng, Z. Xie, L. Wang, X. Jing, F. Wang, *Chem. Asian. J.* **2011**, *6*, 1372; c) L. Chen, Z. Ma, J. Ding, L. Wang, X. Jing, F. Wang, *Chem. Commun.* **2011**, *47*, 9519.

[18] a) H.-H. Chou, H.-H. Shih, C.-H. Cheng, *J. Mater. Chem.* **2010**, *20*, 798; b) J. H. Park, C. Yun, T.-W. Koh, Y. Do, S. Yoo, M. H. Lee, *J. Mater. Chem.* **2011**, *21*, 5422; c) P. Moonsin, N. Prachumrak, R. Rattanawan, T. Keawin, S. Jungsuttiwong, T. Sudyoadsuk, V. Promarak, *Chem. Commun.* **2012**, *48*, 3382.

[19] M. Sudhakar, P. I. Djurovich, T. E. Hogen-Esch, M. E. Thompson, *J. Am. Chem. Soc.* **2003**, *125*, 7796.

[20] S. O. Jeon, K. S. Yook, C. W. Joo, J. Y. Lee, *Adv. Funct. Mater.* **2009**, *19*, 3644.

[21] R. J. Holmes, S. R. Forrest, Y. J. Tung, R. C. Kwong, J. J. Brown, S. Garon, M. E. Thompson, *Appl. Phys. Lett.* **2003**, *82*, 2422.

[22] J. Ding, J. Gao, Y. Cheng, Z. Xie, L. Wang, D. Ma, X. Jing, F. Wang, *Adv. Funct. Mater.* **2006**, *16*, 575.

[23] J. Ding, J. Gao, Q. Fu, Y. Cheng, D. Ma, L. Wang, *Synth. Met.* **2005**, *155*, 539.

[24] A. Endo, K. Sato, K. Yoshimura, T. Kai, A. Kawada, H. Miyazaki, C. Adachi, *Appl. Phys. Lett.* **2011**, *98*, 083302.

[25] K. S. Yook, S. E. Jang, S. O. Jeon, J. Y. Lee, *Adv. Mater.* **2010**, *22*, 4479.

[26] a) S. O. Jeon, K. S. Yook, C. W. Joo, J. Y. Lee, *Appl. Phys. Lett.* **2009**, *94*, 013301; b) J. Lee, J.-I. Lee, J. Y. Lee, H. Y. Chu, *Org. Electron.* **2009**, *10*, 1529.

[27] S. O. Jeon, S. E. Jang, H. S. Son, J. Y. Lee, *Adv. Mater.* **2011**, *23*, 1436.

[28] S. J. Su, T. Chiba, T. Takeda, J. Kido, *Adv. Mater.* **2008**, *20*, 2125.

[29] B. Zhang, L. Liu, G. Tan, B. Yao, C.-L. Ho, S. Wang, J. Ding, Z. Xie, W.-Y. Wong, L. Wang, *J. Mater. Chem. C* **2013**, 1, 4933.

[30] a) B. Chen, J. Ding, L. Wang, X. Jing, F. Wang, *J. Mater. Chem.* **2012**, *22*, 23680; b) T. Peng, G. Li, K. Ye, C. Wang, S. Zhao, Y. Liu, Z. Hou, Y. Wang, *J. Mater. Chem. C* **2013**, *1*, 2920.

[31] P. Schrogel, A. Tomkeviciene, P. Strohriegl, S. T. Hoffmann, A. Kohler, C. Lennartz, *J. Mater. Chem.* **2011**, *21*, 2266.